

Targeted Disruption of *Hotair* Leads to Homeotic Transformation and Gene Derepression

Lingjie Li,¹ Bo Liu,^{2,4} Orly L. Wapinski,^{1,4} Miao-Chih Tsai,^{1,4} Kun Qu,¹ Jiajing Zhang,¹ Jeff C. Carlson,² Meihong Lin,¹ Fengqin Fang,³ Rajnish A. Gupta,¹ Jill A. Helms,² and Howard Y. Chang^{1,*}

¹Howard Hughes Medical Institute and Program in Epithelial Biology, Stanford University School of Medicine, Stanford, CA 94305, USA

²Department of Surgery, Stanford University School of Medicine, Stanford, CA 94305, USA

³Division of Immunology and Rheumatology, Department of Medicine, Stanford University School of Medicine, Stanford, CA 94305, USA

⁴These authors contributed equally to this work

*Correspondence: howchang@stanford.edu

<http://dx.doi.org/10.1016/j.celrep.2013.09.003>

This is an open-access article distributed under the terms of the Creative Commons Attribution-NonCommercial-No Derivative Works License, which permits non-commercial use, distribution, and reproduction in any medium, provided the original author and source are credited.

SUMMARY

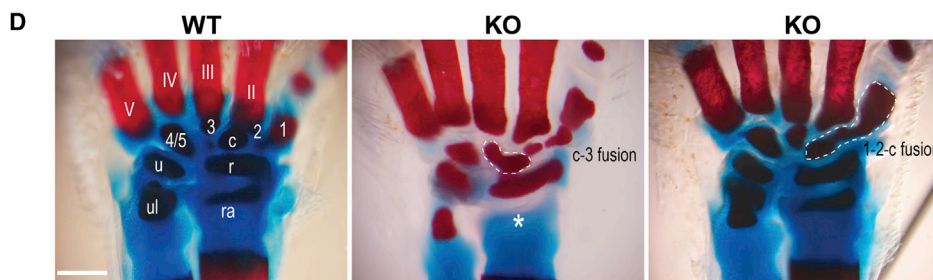
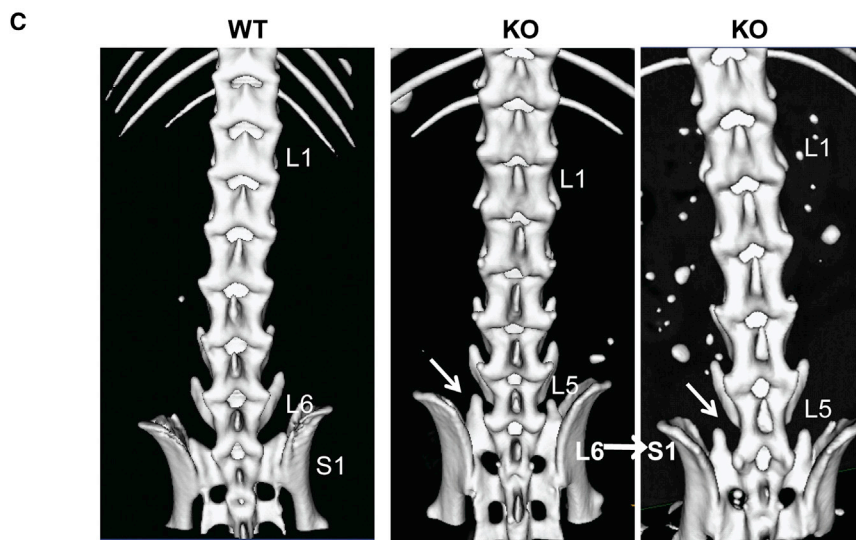
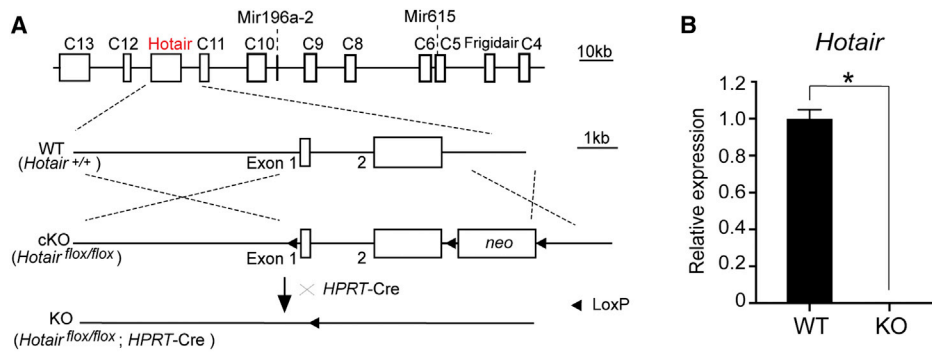
Long noncoding RNAs (lncRNAs) are thought to be prevalent regulators of gene expression, but the consequences of lncRNA inactivation *in vivo* are mostly unknown. Here, we show that targeted deletion of mouse *Hotair* lncRNA leads to derepression of hundreds of genes, resulting in homeotic transformation of the spine and malformation of metacarpal-carpal bones. RNA sequencing and conditional inactivation reveal an ongoing requirement of *Hotair* to repress *HoxD* genes and several imprinted loci such as *Dlk1-Meg3* and *Igf2-H19* without affecting imprinting choice. *Hotair* binds to both Polycomb repressive complex 2, which methylates histone H3 at lysine 27 (H3K27), and Lsd1 complex, which demethylates histone H3 at lysine 4 (H3K4) *in vivo*. *Hotair* inactivation causes H3K4me3 gain and, to a lesser extent, H3K27me3 loss at target genes. These results reveal the function and mechanisms of *Hotair* lncRNA in enforcing a silent chromatin state at *Hox* and additional genes.

INTRODUCTION

Long noncoding RNAs (lncRNAs) are pervasively transcribed in mammalian genomes (reviewed by Rinn and Chang, 2012). Thousands of lncRNA species have been reported, but their *in vivo* functions are mostly unknown. Some lncRNAs act at the interface between the genome and chromatin modification machinery, such as Xist and Air that recruit repressive chromatin modifications to silence nearby genes in *cis* for dosage compensation and imprinting (Lee, 2009; Nagano et al., 2008). Other lncRNAs, such as HOTAIR and linc-p21, act in *trans* to guide silencing complexes to sites throughout the genome (Huarte et al., 2010; Rinn et al., 2007). Histone H3 lysine 27 trimethylation (H3K27me3) mediates developmental silencing, whereas histone H3 lysine 4 trimethylation

(H3K4me3) is associated with transcriptional activation. Human HOTAIR, a 2.2 kb RNA transcribed from the *HOXC* locus, binds both Polycomb repressive complex 2 (PRC2) and LSD1 complexes and recruits them to hundreds of genomic sites to promote coordinated H3K27 methylation and H3K4 demethylation, respectively, for gene silencing (Chu et al., 2011; Rinn et al., 2007; Tsai et al., 2010). HOTAIR silences human *HOXD* genes, a function that is believed to contribute to cell positional identity (Rinn et al., 2007), and overexpression of HOTAIR in several types of human cancers has been linked to metastasis and cancer progression (Gupta et al., 2010; Kim et al., 2013; Kogo et al., 2011). HOTAIR has been considered a prototype of lncRNA-guided chromatin modification that typifies a large class of lncRNAs associated with PRC2 and other chromatin modification complexes (Khalil et al., 2009; Zhao et al., 2010).

The evolutionary conservation of lncRNA sequence and function is potentially distinct from that of protein-coding genes (Derrien et al., 2012; Ulitsky et al., 2011). Although lncRNAs show greater sequence conservation than introns, even functionally redundant lncRNAs exhibit only limited sequence identity (e.g., roX RNAs in *Drosophila*). lncRNAs show greater conservation of genomic synteny than sequence identity (Ulitsky et al., 2011). These findings raise the possibility that functional lncRNAs may quickly arise in evolution but also suggest that understanding lncRNA function across evolution likely requires direct experimental analysis. Mouse *Hotair* (hereafter *Hotair*) is a lncRNA transcribed from the syntenic location in the *HoxC* locus and is expressed in posterior or distal anatomic sites (Rinn et al., 2007; Schorderet and Duboule, 2011). Analysis of a large deletion of mouse *HoxC* locus (*HoxCΔ* [Suemori and Noguchi, 2000], which includes *Hotair*) found little change in *HoxD* gene expression or chromatin state, which led to the interpretation that mouse and human *Hotair* are functionally distinct (Schorderet and Duboule, 2011). However, because *HoxCΔ* also removes eight *HoxC* genes, two microRNAs, and additional lncRNAs, its use to assign function to *Hotair* may be less than ideal. Here, we generate and analyze the targeted deletion of *Hotair* and discover its function in modulating the chromatin state and gene expression of *HoxD* and imprinted genes *in vivo*.



E Skeletal abnormalities in *Hotair* KO mice:

Phenotype	Penetrance of skeletal abnormalities		
	KO	WT	p Value
Lumbar-sacral transition (L6 → S1)	58% (n=31)	6% (n=18)	0.0002
Wrist defects	56% (n=18)	9% (n=11)	0.019
Caudal transformation (C4)	100% (n=11)	0% (n=5)	0.0002

(legend on next page)

RESULTS

Hotair Knockout Causes Homeotic Transformation and Skeletal Malformation

We first examined *Hotair* expression in developing embryos at embryonic day 11.5 (E11.5), E12.5, and E13.5 stages by in situ hybridization. *Hotair* is specifically expressed in the posterior trunk and distal limb bud (Figure S1A), as previously described by Rinn et al. (2007) and Schorderet and Duboule (2011). *Hotair* is expressed from somites 33–34 onward posteriorly, corresponding to the developing lumbosacral anatomical region. *Hotair* is also expressed in specific mesenchymal cells and condensates in E11.5 and E15.5 forelimb, including wrist and digital condensates (Figures S1B and S1C). The site-specific expression pattern of *Hotair* suggests potential roles in vertebrae and wrist morphogenesis during development.

To understand the functions of mouse *Hotair*, we generated conditional and constitutive knockout (KO) alleles of the *Hotair* locus (Figure 1A; Experimental Procedures). We introduced LoxP sites to flank exons 1 and 2, which comprise the entirety of the known *Hotair* transcript; crossing to *HPRT*-Cre mice (activating Cre in female germline) yielded targeted deletion of the locus (hereafter “*Hotair* KO”) and resulted in no detectable *Hotair* RNA expression (Figures 1B and S1D). *Hotair* KO allele was backcrossed to C57/BL6 background for six generations, yielding over 99% C57/BL6 background as confirmed by strain-specific SNP array analysis (Experimental Procedures). Heterozygous intercrosses generated *Hotair* wild-type (WT) and KO littermates for comparison.

Homozygous *Hotair* KO animals were viable and fertile but showed three notable skeletal phenotypes (Figures 1C–1E, S1E, and S1F). First, in the C57/BL6 genetic background, WT littermates possess six lumbar vertebrae (L1–L6); whereas 58% of *Hotair* KO mice have five lumbar vertebrae ($p = 0.0002$, Fisher’s exact test). Microscale computed tomography (micro-CT) revealed that the sacral 1 (S1) vertebrae in *Hotair* KO still had the lateral processes typical of L6 vertebrae, indicative of a L6 to S1 transformation (Figure 1C). These micro-CT findings were confirmed by Alcian blue staining of the vertebral skeleton (Figure S1E). Second, detailed examination of the limb skeleton also revealed a majority of KOs (56% versus 9% in WT) with abnormalities in the metacarpal and carpal bones, including fusions and missing bony elements (Figures 1D and 1E). The spine and wrist abnormalities do not necessarily co-occur in individual animals; hence, up to 78% of KO animals exhibit one or more of these abnormalities. Third, *Hotair* KO animals exhibited a subtle but fully penetrant transformation of the caudal

4 vertebrae (Figures 1E and S1F). These phenotypes were robust through all the backcrosses, and we never saw the phenotype segregate independently from the *Hotair* allele. These results suggest that *Hotair*, first identified in the context of adult skin positional identity (Rinn et al., 2007), is also important for embryonic patterning of the skeletal system in vivo.

Gene Derepression in *Hotair* KO Cells and Embryos

We analyzed gene expression patterns in *Hotair* KO to gain insights into the molecular basis for the observed phenotypes. Although *Hotair* expression is segment specific and heterogeneous in embryos and mouse embryonic fibroblasts (MEFs), we found that primary tail tip fibroblasts (TTFs, derived from a posterior site where *Hotair* is highly expressed) maintained position-specific and consistent *Hotair* expression (Figures S2A and S2B). Single-cell analysis shows that the vast majority of individual TTF cells (83%) express *Hotair*, whereas only 28% of MEF cells express *Hotair* (Figure S2C). The enrichment of a relatively pure population of *Hotair*⁺ cells is ideal to address the impact of *Hotair* KO at the molecular level. Previous studies with human HOTAIR used RNAi, which were not able to fully deplete HOTAIR (Rinn et al., 2007; Tsai et al., 2010). Hence, the consequences of targeted and complete *Hotair* inactivation on gene expression are not known. RNA sequencing (RNA-seq) of TTFs derived from WT, heterozygous, and *Hotair* KO mice revealed significant differences in expression (Figure 2A). Validation by microarray analysis and quantitative RT-PCR (qRT-PCR) of TTFs from independent animals yielded genes with consistent expression changes in multiple platforms that we consider *Hotair*-dependent target genes (Figure S2D).

Hotair KO resulted in predominantly derepression of gene expression. Approximately 80% of the gene expression changes are increased in the KO cells, suggesting that *Hotair* functions primarily as a repressor, either directly or indirectly. Prominent among the derepressed genes are several *HoxD* genes, including *Hoxd10*, *Hoxd11*, and *Hoxd13* (Figures 2A and 2B). Multiple *HoxC* genes are expressed and well detected, but no significant difference in *HoxC* expression level was observed despite the fact that *Hotair* is embedded in the *HoxC* locus (Figure S2F). In addition, gene expression from *HoxA* and *HoxB* loci was not significantly affected (Figure S2F). Thus, similar to human HOTAIR, mouse *Hotair* appears to be a *trans*-acting regulator of gene expression.

Moreover, *Hotair* KO increased the expression of approximately 30 genes from imprinted loci. These include paternally expressed genes *Dlk1*, *Dio3*, *Igf2*, *Mest*, and *Slc38a4* (Figure 2A, blue) and maternally expressed genes *H19* and *Meg3* (also

Figure 1. *Hotair* KO Causes Homeotic Transformations

(A) Schematic of *Hotair* cKO allele is shown. Arrowhead points to LoxP site.

(B) qRT-PCR confirms loss of *Hotair* expression in KO TTF. Mean \pm SD is shown ($n > 3$). * $p < 0.05$, Student’s t test.

(C) Micro-CT scans show “L6 \rightarrow S1” homeotic transformation of the lumbar vertebrae, which resulted in losing the sixth lumbar and having structurally deformed first sacral vertebrae (arrow) in *Hotair* KO mice. L, lumbar vertebrae; S, sacral vertebrae.

(D) Alizarin red-Alcian blue staining shows the deformed wrist bones in KO mice. Digits are indicated as II–V, and carpal elements as 1, 2, 3, and 4/5. c, central element; r, radiale; u, ulnare; ra, radius; ul, ulna. Note the fusion of carpal elements c-3 and 1-2-c (circled area), and missing radius (asterisk) in KOs. Carpal elements 4/5 are always naturally fused in WT wrist. Scale bar, 0.5 mm.

(E) Summary of skeletal abnormalities in *Hotair* KO mice is presented. Phenotype penetrance, number (n) of animals examined, and p values (Fisher’s exact test) are indicated.

See also Figure S1.

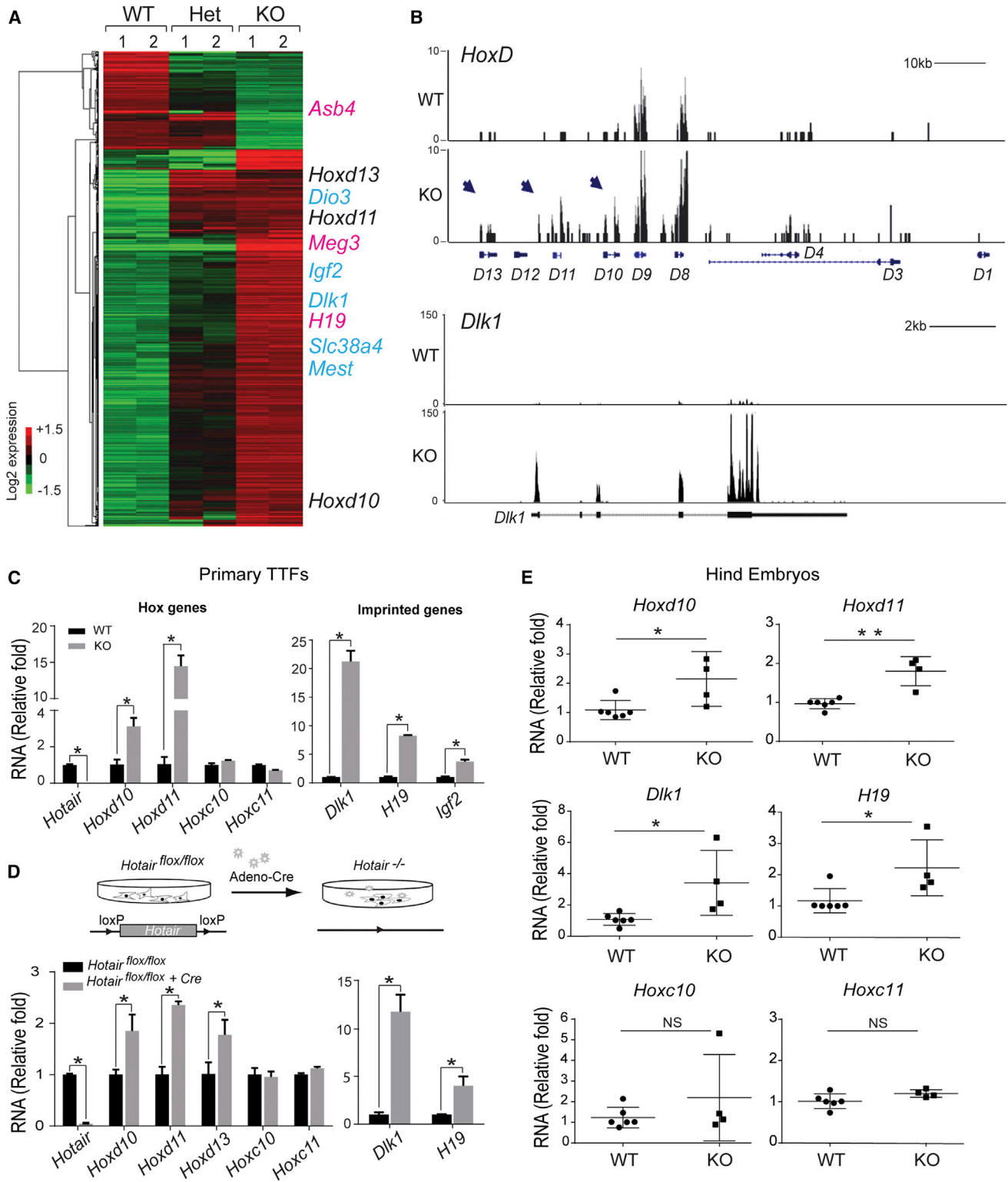


Figure 2. *Hotair* KO Derepresses *HoxD* and Imprinted Genes

(A) Differential gene expression by RNA-seq in *Hotair* WT, heterozygous (Het), and KO TTF is shown. Each row is a transcript; each column is a sample. Derepressed *HoxD* (black) and imprinted genes (maternally expressed is indicated in pink; paternally expressed is in blue) are indicated.

(B) RNA-seq data of *HoxD* and *Dlk1* loci are presented. Distal *HoxD* genes (*D13*, *D11*, and *D10*, indicated by the arrow) and *Dlk1* were derepressed in KO cells.

x axis shows the genomic coordinate; y axis shows the normalized RNA-seq signals. Box represents known mRNA exons.

(legend continued on next page)

known as *Gtl2*) (Figure 2A, pink). Genes surrounding the imprinted loci were not affected (Figures 2B and S2F). Although only a minority of all known imprinted genes was derepressed, we noted that the affected genes tend to be clustered in chromosomal loci (Figure S2F). For example, *Dlk1*, *Meg3*, and *Dio3* reside in the same imprinted locus on mouse chromosome 12 (da Rocha et al., 2009; Takahashi et al., 2009). Notably, partial derepression of *HoxD* genes is observed in *Hotair*^{+/-} cells, whereas derepression of imprinted genes was only observed in the *Hotair* KO cells. This result suggests that the effect of *Hotair* on *HoxD* genes may be dose dependent and potentially explains why prior studies knocking down HOTAIR did not observe effects on imprinted genes.

Genes with altered expression had significant enrichment for Gene Ontology terms related to transcriptional regulation, cell proliferation, and development ($p < 0.05$ for each; FDR < 0.05 ; Figure S2E). qRT-PCR of independent TTF cells from WT and *Hotair* KO mice confirmed the derepression of multiple *HoxD* and imprinted genes, but no significant changes in *Hoxc10* and *Hoxc11* (Figure 2C). *Hoxd11* is induced over 10-fold and is the most strongly derepressed gene among the *HoxD* genes. *Dlk1*, *H19*, and *Igf2* are also derepressed from 5- to over 20-fold in *Hotair* KO tissue. Fluorescence-activated cell sorting (FACS) and immunofluorescence staining confirmed the increased synthesis of *Dlk1* and *Igf2* proteins in *Hotair* KO cells (Figures S2G and S2H).

To determine whether ongoing *Hotair* function is required for proper gene expression, we studied the consequences of inducible acute deletion of *Hotair*. Introduction of Cre-expressing adenovirus into *Hotair*^{fllox/fllox} TTFs led to high-efficiency deletion and silencing of *Hotair* expression (Figure 2D). Introduction of control adenovirus served as negative control. Acute deletion of *Hotair* led to derepression of *HoxD* and imprinted genes after three to five passages, albeit with lower-fold effect than the constitutive *Hotair* KO; whereas expression of *Hoxc10* and *Hoxc11* was not affected (Figure 2D). The acute genetic deletion in isogenic cells rules out potential background effects and suggests an ongoing requirement of *Hotair* for proper expression of its target genes in *trans*. qRT-PCR analysis of posterior and distal embryonic tissues, where endogenous *Hotair* is normally expressed, confirmed derepression of *HoxD* and imprinted genes in *Hotair* KO embryos without significant changes in *HoxC* genes (Figure 2E).

Hotair KO Alters Spatial Pattern of Gene Expression In Vivo

Hotair KO alters both the spatial pattern as well as the quantitative levels of gene expression. *Hox* genes are expressed along the anterior-posterior and proximal-distal axis in a nested, segmental fashion related to their positions on the chromosomes (Krumlauf, 1994). Hence, 5' *HoxD* genes are expressed posteriorly and distally, a pattern that requires proper chromatin-based silencing mechanisms such as Polycomb (Soshnikova

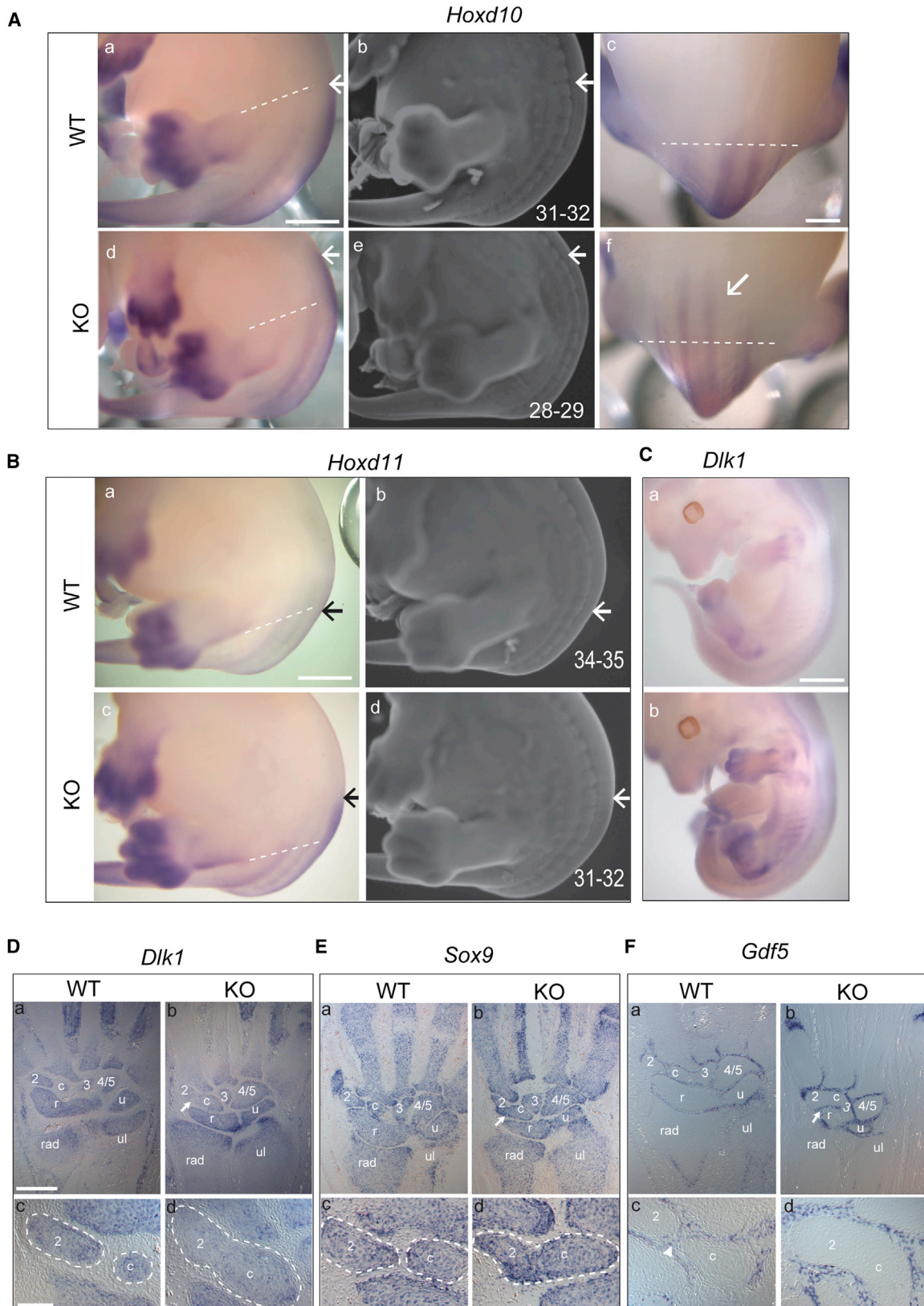
and Duboule, 2009). *Hotair* KO embryos showed anterior expansion of the *Hoxd10*, and *Hoxd11* expression domain in the trunk compared to WT littermates, an effect that is recognizable starting at E12.5 and confirmed by examination of E13.5 embryos (Figures 3A and 3B). The anterior boundary of *Hoxd10* expression is shifted domain from somites 31–32 (WT) to somites 28–29 (KO), and *Hoxd11* domain from somites 34–35 (WT) to somites 31–32 (KO), which are the precursors of the developing lumbosacral vertebrae (Figures 3A and 3B) (Burke et al., 1995). In addition, the level of *Hoxd11* expression in the posterior trunk and distal limb buds was consistently elevated in the *Hotair* KO (Figure 3B). In contrast, *HoxC* genes did not show anteriorization or increased intensity of expression (Figure S3). We also analyzed the expression pattern of the imprinted gene *Dlk1*. Intriguingly, whereas *Dlk1* is under imprinted control in all cells (da Rocha et al., 2008), *Hotair* KO led to ectopic *Dlk1* expression in the posterior trunk and in the distal limbs, which corresponds to the anatomic sites of endogenous *Hotair* expression (Figure 3C).

Detailed examination of the limb suggested a connection between *Dlk1* derepression and wrist skeletal element abnormalities. *Dlk1* functions as a delta-like ligand of the Notch pathway and has been implicated in osteogenesis (Abdallah et al., 2004). At E15.5, *Dlk1* expression is normally confined to the mesenchymal condensation of the wrist bones (Figure 3D). These condensations are also marked by *Sox9* expression and demarcated by *Gdf5*, which is expressed in cells of the perichondrium that later form cortical bone (Bi et al., 1999; Francis-West et al., 1999). We found that *Hotair* KO animals showed expansion of the *Dlk1* expression domain, such that multiple *Sox9*-positive condensations become contiguous, and the intervening *Gdf5*-positive domains are lost (Figures 3D–3F). These results suggest a cell fate switch where a subset of perichondrial cells—destined to form bone—can become cartilage-producing chondrocytes, analogous to mesenchymal fate changes seen with perturbed Wnt or Shh signaling (Day et al., 2005; Niedermaier et al., 2005). The domain of increased *HoxD* expression is much broader in the *Hotair* KO than the site of wrist bone abnormalities; on the other hand, the alteration in *Dlk1* expression tracks closely with the wrist phenotype. Thus, the localized phenotype suggests the involvement of either *Dlk1* alone, or both *Dlk1* and *HoxD* genes. Collectively, these results suggest that *Hotair* is required to silence genes for proper pattern of gene expression in vivo.

Hotair Regulates Histone Modification at Select Loci

Biochemical and functional studies indicate that *Hotair* regulates histone modification patterns genome wide (Figure 4). Because protein partners of mouse *Hotair* are not fully characterized, we examined its association with key chromatin modification complexes. Immunoprecipitation (IP) of PRC2 subunits Ezh2 or Suz12, and separately the histone demethylase Lsd1, from posterior E11.5 embryos specifically retrieved *Hotair* but not Malat1 nor U1 RNA, whereas NF- κ B subunit p65 (also known as RelA)

(C and D) qRT-PCR of indicated genes in *Hotair* KO cells (C) or after acute *Hotair* deletion in cKO cells (D) is shown. Top is a schematic of acute deletion assay. (E) qRT-PCR of indicated genes in *Hotair* KO embryos is presented. The hind portions of E13.5 embryos from the same litters were analyzed ($n > 3$). Mean \pm SD is shown for all panels. * $p < 0.05$ and ** $p < 0.01$ by Student's *t* test ($n > 3$). NS, not significant. See also Figure S2.



(legend on next page)

and control IgG retrieved neither (Figure 4A). This result suggests that Hotair binds both H3K27 methylase and H3K4 demethylase complexes, similar to its human counterpart. *Hotair* KO led to loss of H3K27me3 and gain of H3K4me3 at *HoxD* (including *Hoxd1*, *Hoxd3*, *Hoxd11*, and *Hoxd13*) and imprinted gene loci (such as *Dlk1*, *H19*, *Igf2*, *Plag1*, and *Dcn*), as shown by chromatin IP (ChIP) followed by qPCR in TTFs (Figure 4B). ChIP signal at *Fgf4* was not changed in KO and served as negative control. We also found that PRC2 occupancy at *HoxD* and imprinted genes are significantly reduced in the *Hotair* KO (Figure S4A).

We next analyzed the global pattern of H3K27me3 and H3K4me3 by ChIP sequencing (ChIP-seq). Genes that are derepressed by *Hotair* KO showed, on average, broad decrease of H3K27me3 occupancy and focal gain of H3K4me3 centered around their transcriptional start sites (Figure 4C). Conversely, promoters with Hotair-dependent loss of H3K27me3 or gain of H3K4me3 are significantly enriched for derepressed genes in *Hotair* KO ($p < 0.0001$; gene set enrichment analysis for concordance between each chromatin change and gene induction). Next, we organized the H3K27me3 and H3K4me3 ChIP-seq data by unsupervised hierarchical clustering and displayed the RNA level changes in KO versus WT in parallel (Figure 4D). This analysis revealed two main patterns of histone modification change in association with gene derepression: one cluster of loci (termed cluster i) showed coordinate broad loss of H3K27me3 and focal gain of H3K4me3 in *Hotair* KO; another cluster of loci (termed cluster ii) showed only H3K4me3 gain but lacked H3K27me3 in either WT or KO cells. The two clusters demonstrate comparable levels of gene derepression in *Hotair* KO, but cluster i has a lower level of H3K4me3 in WT cells, consistent with their co-occupancy with H3K27me3. These results suggest that Hotair can regulate coordinated H3K4 and H3K27 methylation at some loci (via both PRC2 and Lsd1) and solely H3K4 methylation at other loci (via Lsd1). Although the emergence of H3K4me3 signal may be due to the well-known association of H3K4me3 with active promoters or secondary effects, the fact that not all loci with H3K4me3 gain showed RNA increase suggests that H3K4me3 gain in KO cells is not simply a consequence of increased transcription. Additional genes derepressed in *Hotair* KO are associated with different and heterogeneous chromatin patterns, which may occur through alternative or indirect mechanisms.

Because DNA methylation is a well-studied regulator of imprinting status (Abramowitz and Bartolomei, 2012), we tested whether Hotair may also influence DNA cytosine methylation. Bisulfite conversion and sequencing of the intergenic differentially methylated region (IG-DMR) from *Dlk1-Gtl2* locus showed

that deletion of *Hotair* had no significant impact on DNA methylation at this locus (Figure S4B). These results suggest that Hotair affects the *Dlk1* locus principally through control of histone methylation genome wide.

DISCUSSION

lncRNAs are increasingly recognized as potential mediators of gene regulation and pathogenic loci in human diseases (Rinn and Chang, 2012). Hence, there is an important need to understand their physiological functions in model organisms. The targeted and conditional KO (cKO) of *Hotair* provides a model to analyze lncRNA functions in vivo for development and cancer. Human HOTAIR was the first lncRNA reported to silence genes in *trans*, notably *HOXD* genes (Rinn et al., 2007). *Hotair* KO is now shown to cause derepression at multiple genes, including *Hoxd10* and *Hoxd11*, which are important for patterning of lumbosacral junction and of metacarpal and carpal bones in the limbs (Favier et al., 1995; Gérard et al., 1996). *Hotair* KO causes increased expression and anterior expansion of *Hoxd10* and *d11* domains, which increases the dosage of *Hoxd* genes in posterior embryo. Notably, L6→S1 transformation is the same phenotype that is observed when ectopic copies of the *HoxD* locus are introduced into mouse genome (Spitz et al., 2001) or when endogenous *Hoxd10* and *Hoxd11* expression domains are anteriorized by deletion of *cis* repressor element (Gérard et al., 1996). These findings suggest that derepression of *Hoxd10* and *Hoxd11* likely contributes to the homeotic axial transformation in *Hotair* KO mice. In silico analyses suggest that Hotair is conserved predating the eutherian-marsupial split, but Hotair is conserved in gene synteny and RNA structure rather than primary sequence (He et al., 2011; Yu et al., 2012). The similar roles of human and mouse Hotair on *HoxD* provide another example of conservation of lncRNA function at syntenic locations despite limited sequence conservation (Ulitsky et al., 2011). This knowledge sets the stage for potential in silico analyses to highlight conserved RNA domains for Hotair function, and phenotypic rescue of *Hotair* KO with human HOTAIR and mutants should provide definitive structure-function studies.

Because some homeotic transformations occur with different frequency in different genetic backgrounds, care and proper controls are important to interpret this result. After extensive backcrossing to homogeneous genetic background, *Hotair* KO demonstrated significantly increased (~10-fold) L6→S1 transformation compared to WT littermates. Moreover, inducible deletion of *Hotair* in isogenic cells also derepressed *HoxD* and *Dlk1*, suggesting that these are direct effects of Hotair removal.

Figure 3. Spatial and Temporal Gene Expression Patterns in *Hotair* KO Mice

(A and B) Whole-mount in situ hybridization (WISH) of *Hoxd10* (Aa, Ac, Ad, and Af) and *Hoxd11* (Ba and Bc) of E13.5 embryos ($n > 3$ for each genotype) is shown. KO embryos showed increased intensity and anterior shift of the expression domains of *HoxD* genes (highlighted with arrows; the dotted lines across hindlimbs are used as anatomical limit). The same embryos were costained with ethidium bromide, and the somite position of the anterior expression domain was numbered and marked with arrows (Ab, Ae, Bb, and Bd). Scale bars, 1 mm (Aa, Ab, Ad, Ae, and Ba–Bd) and 600 μ m (Ac and Af).

(C) WISH of *Dlk1* on E12.5 embryos shows ectopic expression in *Hotair* KO embryos. (WT, $n = 4$; KO, $n = 5$). Scale bar, 1 mm.

(D–F) Altered *Dlk1* expression and mesenchymal cell fates in *Hotair* KO wrists are shown. *Dlk1* (D), *Sox9* (E), and *Gdf5* (F) expression in E15.5 wrist sections ($n > 3$ for each genotype) is presented. Arrows indicate the joint regions in KO. Dotted circles mark the carpal element 2 and central element. Arrowhead indicates the intervening *Gdf5*-positive domain in WT. Note 2-c fusion in KO wrist, showing continuous *Dlk1* and *Sox9* expression in the junction area of 2 and c; and loss of *Gdf5* signal as well. Scale bars, 300 μ m (Da, Db, Ea, Eb, Fa, and Fb) and 100 μ m (Dc, Dd, Ec, Ed, Fc, and Fd).

See also Figure S3.

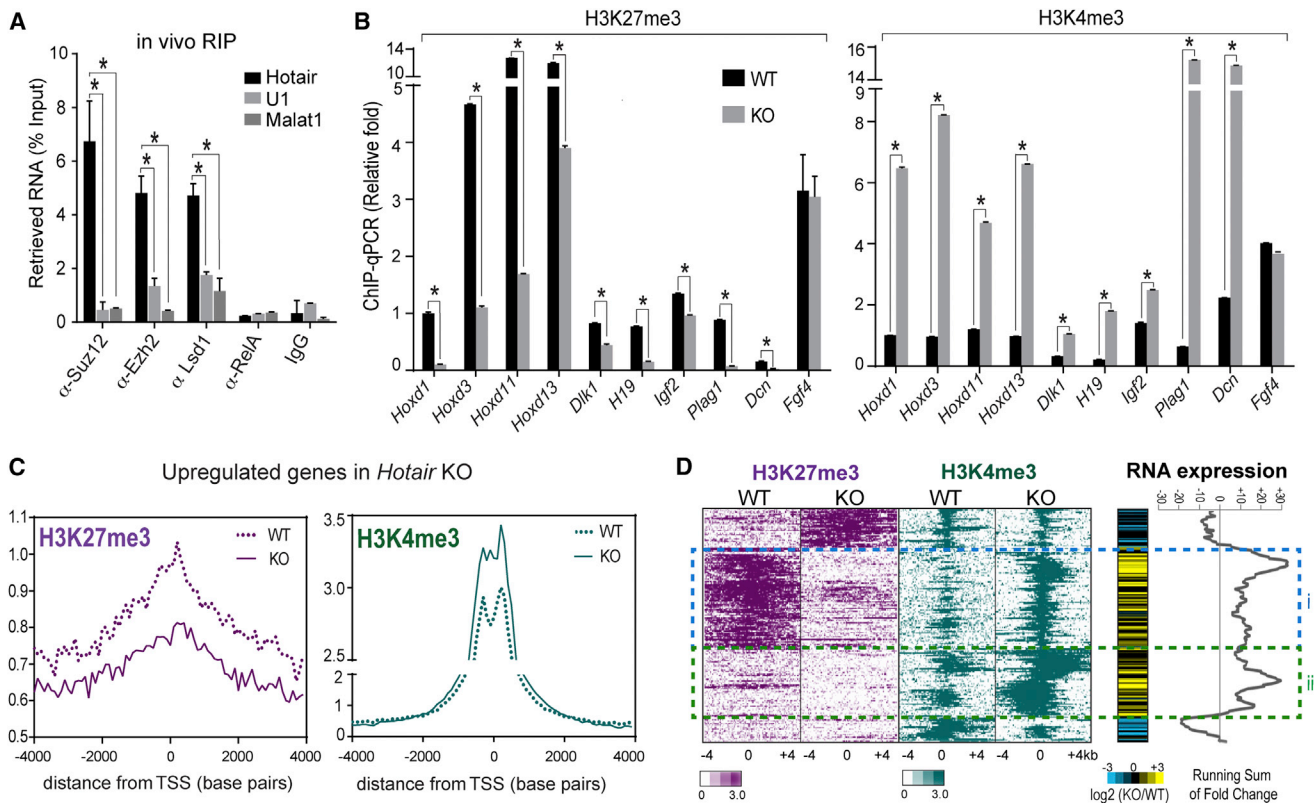


Figure 4. *Hotair* Regulates Silent Chromatin State Genome Wide

(A) *Hotair* binds PRC2 and Lsd1 complexes in vivo. RNA-IP (RIP) of E11.5 embryos with the indicated antibodies was followed by qRT-PCR of *Hotair* and control RNAs (U1, Malat1) and normalized with 1% input performed in parallel (n = 3).

(B) ChIP-qPCR in *Hotair* KO versus WT cells of H3K27me3 (left panel) and H3K4me3 (right panel) of the indicated genes is presented. *Fgf4* was not changed in KO and served as a negative control (n = 3).

(C) Average H3K27me3 (left panel) and H3K4me3 (right panel) ChIP-seq signal across the transcription start site (TSS) of upregulated genes in *Hotair* KO cells is shown.

(D) Relationship of histone modifications to gene derepression in *Hotair* WT and KO cells is presented. Heatmap zoom-in of ChIP-seq signal in 8 kb bins centered on peak summits after unsupervised hierarchical clustering (left) is shown. RNA expression changes (KO/WT) and running sums across clusters are shown (right). Gene activation is seen in cluster i (75 loci) with both H3K27me3 loss and H3K4me3 gain; cluster ii shows 70 loci with only H3K4me3 gain in *Hotair* KO.

Mean ± SD is shown for all panels. *p < 0.05, Student's t test.

See also Figure S4.

However, the frequency of the L6 transition in *Hotair* KO (58%) is less than that observed in *HoxD* transgene (>80%) or derepression in *cis* (~100%) (Gérard et al., 1996; Spitz et al., 2001). These differences may be due to less-potent regulation in *trans* versus in *cis*, potential redundancy in recruitment mechanisms of silencing complexes, or different genetic backgrounds.

An intriguing question is why *HoxCΔ* did not reveal a more drastic phenotype. Schorderet and Duboule also observed that *Hoxd8*, *d9*, and *d10* are derepressed by approximately 2-fold in *HoxCΔ* compared to WT (Schorderet and Duboule, 2011), but these changes were not apparently sufficient to cause skeletal transformations. Reanalysis of the published RNA-seq data from *HoxCΔ* (Schorderet and Duboule, 2011) revealed modest but consistent upregulation of all three remaining *Hox* loci, such that the total dosage of *Hox* transcripts is maintained in *HoxCΔ* tissue (Figures S4C and S4D). This finding may also explain why *HoxCΔ* has a milder phenotype than deletions of individual *HoxC* genes (Suemori and Noguchi, 2000). Alternatively,

HoxCΔ may remove genes with functions antagonistic to *Hotair*, which are preserved in *Hotair* KO. Although not detected in the tissues and time points examined, we cannot rule out the possibility that *Hotair* affects one or more *Hoxc* gene in *cis* at other times in development, which would be absent in *HoxCΔ*. The comparison between *HoxCΔ* and targeted *Hotair* KO also demonstrates the value of multiple and fine-scale manipulations to define lncRNA function in vivo.

Hotair KO reveals an unexpected role for *Hotair* in transcriptional repression of several imprinted gene loci. Imprinting involves the selective expression of genes between two nearly identical copies, the paternal versus maternal alleles; similarly, developmental *Hox* expression involves the selective expression from among highly homologous copies of homeodomain genes, from the *Hox* loci. Beyond these conceptual parallels, our results suggest a direct cross-regulation between *Hox* and some imprinted loci. The diversity of imprinting mechanisms potentially explains why *Hotair* KO only affects the expression of a small

subset of imprinted genes. *Hotair* is likely to be involved in the maintenance of proper gene expression levels rather than the initial imprint choice because (1) *Hotair* is not expressed in early zygotes when imprinted alleles are marked by DNA methylation, and (2) DNA methylation of the imprinted loci (which reflect imprinting choice) is not altered in *Hotair* KO. Consistently, *Hotair* KOs do not demonstrate phenotypes of complete imprinting loss, such as postnatal lethality from altered dosages of the *Dlk1* locus (da Rocha et al., 2009; Takahashi et al., 2009). The role of *Hotair* may be similar to that of *Bmi1*, a Polycomb protein that controls the expression level, but not the imprinting choice, of multiple imprinted genes to regulate self-renewal of adult stem cells (Zacharek et al., 2011). In an analogous fashion, *Hotair* controls Polycomb- and *Lsd1*-related histone modification state to repress several imprinted genes; alteration of imprinted genes and, consequently, stem cell self-renewal provide potentially new insights for human cancers that overexpress HOTAIR (Gupta et al., 2010; Kim et al., 2013; Kogo et al., 2011).

The set of genes that show altered expression or chromatin state may represent direct or indirect effects of *Hotair* KO. Delineating the direct targets of *Hotair*, such as by chromatin isolation by RNA purification (Chu et al., 2011), will be an important future direction. The ability of *Hotair* to affect the chromatin state may arise from direct regulation or be due to the known physical clustering and mutual influence of the epigenetic states of some imprinted gene loci (Sandhu et al., 2009). The generation of *Hotair* cKO allows these and other potential mechanisms to be dissected in future studies.

EXPERIMENTAL PROCEDURES

Detailed experimental and analysis methods can be found in [Extended Experimental Procedures](#).

Animals

Hotair cKO mice were generated by homologous recombination and were crossed to *HPRT-Cre* mice to yield ubiquitous deletion of the *Hotair* Locus.

All the mice were bred in the Stanford University Research Animal Facility in accordance with the guidelines (see details in [Extended Experimental Procedures](#)).

RNA-Seq

Poly-A-selected RNA was isolated from the fibroblast of *Hotair* WT, heterozygous, and KO mice. The libraries were prepared with the dUTP protocol and sequenced using the Illumina Genome Analyzer IIX platform with 36 bp reads. Raw reads were aligned to the mouse reference sequences NCBI Build 37/mm9 with the TopHat (v.1.1.3) algorithm. Expression levels of RefSeq annotated genes were calculated in unit of reads per kilobase of exon model per million mapped fragments (RPKM). Detailed analysis is presented in [Extended Experimental Procedures](#).

ChIP-Seq and ChIP-qPCR

ChIP-qPCR and ChIP-seq were performed as described (Tsai et al., 2010). Sequencing libraries were made following Illumina's protocol. qPCR analysis was performed with Roche's LightCycler. Sequencing reads (36 bp) were generated on Illumina GAIIX Genome Analyzer and were uniquely mapped to mouse reference genome (NCBI37/mm9) using Bowtie (version 0.12.6). Peaks for each sample were called using MACS algorithm (version 1.4.2). Detailed analysis is presented in [Extended Experimental Procedures](#).

ACCESSION NUMBERS

The GEO accession number for all genomic data herein is GSE48007.

SUPPLEMENTAL INFORMATION

Supplemental Information includes Extended Experimental Procedures and four figures and can be found with this article online at <http://dx.doi.org/10.1016/j.celrep.2013.09.003>.

ACKNOWLEDGMENTS

We thank D. Friendewey and V. Lai for communicating unpublished observations of the C4 vertebrae, members of the H.Y.C. lab and A. Oro for discussion, the Stanford Small Animal Imaging Facility for micro-CT analysis, P. Schorderet and D. Duboule for *HoxCΔ* RNA-seq data and reagents, E. Zelzer for reagents, and P. Grote for in vivo RIP protocol. This work was supported by the NIH (R01-CA118750 to H.Y.C.), the National Science Foundation (to O.L.W.), and the Susan G. Komen Foundation (to M.-C.T.). H.Y.C. is an Early Career Scientist of the Howard Hughes Medical Institute.

Received: July 30, 2013

Revised: August 30, 2013

Accepted: September 2, 2013

Published: September 26, 2013

REFERENCES

- Abdallah, B.M., Jensen, C.H., Gutierrez, G., Leslie, R.G., Jensen, T.G., and Kassem, M. (2004). Regulation of human skeletal stem cells differentiation by *Dlk1*/Pref-1. *J. Bone Miner. Res.* *19*, 841–852.
- Abramowitz, L.K., and Bartolomei, M.S. (2012). Genomic imprinting: recognition and marking of imprinted loci. *Curr. Opin. Genet. Dev.* *22*, 72–78.
- Bi, W., Deng, J.M., Zhang, Z., Behringer, R.R., and de Crombrugge, B. (1999). *Sox9* is required for cartilage formation. *Nat. Genet.* *22*, 85–89.
- Burke, A.C., Nelson, C.E., Morgan, B.A., and Tabin, C. (1995). *Hox* genes and the evolution of vertebrate axial morphology. *Development* *121*, 333–346.
- Chu, C., Qu, K., Zhong, F.L., Artandi, S.E., and Chang, H.Y. (2011). Genomic maps of long noncoding RNA occupancy reveal principles of RNA-chromatin interactions. *Mol. Cell* *44*, 667–678.
- da Rocha, S.T., Edwards, C.A., Ito, M., Ogata, T., and Ferguson-Smith, A.C. (2008). Genomic imprinting at the mammalian *Dlk1*-*Dio3* domain. *Trends Genet.* *24*, 306–316.
- da Rocha, S.T., Charalambous, M., Lin, S.P., Gutteridge, I., Ito, Y., Gray, D., Dean, W., and Ferguson-Smith, A.C. (2009). Gene dosage effects of the imprinted delta-like homologue 1 (*dlk1/pref1*) in development: implications for the evolution of imprinting. *PLoS Genet.* *5*, e1000392.
- Day, T.F., Guo, X., Garrett-Beal, L., and Yang, Y. (2005). *Wnt*/beta-catenin signaling in mesenchymal progenitors controls osteoblast and chondrocyte differentiation during vertebrate skeletogenesis. *Dev. Cell* *8*, 739–750.
- Derrien, T., Johnson, R., Bussotti, G., Tanzer, A., Djebali, S., Tilgner, H., Guernec, G., Martin, D., Merkel, A., Knowles, D.G., et al. (2012). The GENCODE v7 catalog of human long noncoding RNAs: analysis of their gene structure, evolution, and expression. *Genome Res.* *22*, 1775–1789.
- Favier, B., Le Meur, M., Chambon, P., and Dollé, P. (1995). Axial skeleton homeosis and forelimb malformations in *Hoxd-11* mutant mice. *Proc. Natl. Acad. Sci. USA* *92*, 310–314.
- Francis-West, P.H., Abdelfattah, A., Chen, P., Allen, C., Parish, J., Ladher, R., Allen, S., MacPherson, S., Luyten, F.P., and Archer, C.W. (1999). Mechanisms of GDF-5 action during skeletal development. *Development* *126*, 1305–1315.
- Gérard, M., Chen, J.Y., Gronemeyer, H., Chambon, P., Duboule, D., and Zákány, J. (1996). In vivo targeted mutagenesis of a regulatory element required for positioning the *Hoxd-11* and *Hoxd-10* expression boundaries. *Genes Dev.* *10*, 2326–2334.
- Gupta, R.A., Shah, N., Wang, K.C., Kim, J., Horlings, H.M., Wong, D.J., Tsai, M.C., Hung, T., Argani, P., Rinn, J.L., et al. (2010). Long non-coding RNA HOTAIR reprograms chromatin state to promote cancer metastasis. *Nature* *464*, 1071–1076.

- He, S., Liu, S., and Zhu, H. (2011). The sequence, structure and evolutionary features of HOTAIR in mammals. *BMC Evol. Biol.* *11*, 102.
- Huarte, M., Guttman, M., Feldser, D., Garber, M., Koziol, M.J., Kenzelmann-Broz, D., Khalil, A.M., Zuk, O., Amit, I., Rabani, M., et al. (2010). A large intergenic noncoding RNA induced by p53 mediates global gene repression in the p53 response. *Cell* *142*, 409–419.
- Khalil, A.M., Guttman, M., Huarte, M., Garber, M., Raj, A., Rivea Morales, D., Thomas, K., Presser, A., Bernstein, B.E., van Oudenaarden, A., et al. (2009). Many human large intergenic noncoding RNAs associate with chromatin-modifying complexes and affect gene expression. *Proc. Natl. Acad. Sci. USA* *106*, 11667–11672.
- Kim, K., Jutooru, I., Chadalapaka, G., Johnson, G., Frank, J., Burghardt, R., Kim, S., and Safe, S. (2013). HOTAIR is a negative prognostic factor and exhibits pro-oncogenic activity in pancreatic cancer. *Oncogene* *32*, 1616–1625.
- Kogo, R., Shimamura, T., Mimori, K., Kawahara, K., Imoto, S., Sudo, T., Tanaka, F., Shibata, K., Suzuki, A., Komune, S., et al. (2011). Long noncoding RNA HOTAIR regulates polycomb-dependent chromatin modification and is associated with poor prognosis in colorectal cancers. *Cancer Res.* *71*, 6320–6326.
- Krumlauf, R. (1994). Hox genes in vertebrate development. *Cell* *78*, 191–201.
- Lee, J.T. (2009). Lessons from X-chromosome inactivation: long ncRNA as guides and tethers to the epigenome. *Genes Dev.* *23*, 1831–1842.
- Nagano, T., Mitchell, J.A., Sanz, L.A., Pauler, F.M., Ferguson-Smith, A.C., Feil, R., and Fraser, P. (2008). The Air noncoding RNA epigenetically silences transcription by targeting G9a to chromatin. *Science* *322*, 1717–1720.
- Niedermaier, M., Schwabe, G.C., Fees, S., Helmrich, A., Brieske, N., Seemann, P., Hecht, J., Seitz, V., Stricker, S., Leschik, G., et al. (2005). An inversion involving the mouse *Shh* locus results in brachydactyly through dysregulation of *Shh* expression. *J. Clin. Invest.* *115*, 900–909.
- Rinn, J.L., and Chang, H.Y. (2012). Genome regulation by long noncoding RNAs. *Annu. Rev. Biochem.* *81*, 145–166.
- Rinn, J.L., Kertesz, M., Wang, J.K., Squazzo, S.L., Xu, X., Bruggmann, S.A., Goodnough, L.H., Helms, J.A., Farnham, P.J., Segal, E., and Chang, H.Y. (2007). Functional demarcation of active and silent chromatin domains in human HOX loci by noncoding RNAs. *Cell* *129*, 1311–1323.
- Sandhu, K.S., Shi, C., Sjölander, M., Zhao, Z., Göndör, A., Liu, L., Tiwari, V.K., Guibert, S., Emilsson, L., Imreh, M.P., and Ohlsson, R. (2009). Nonallelic transvection of multiple imprinted loci is organized by the H19 imprinting control region during germline development. *Genes Dev.* *23*, 2598–2603.
- Schorderet, P., and Duboule, D. (2011). Structural and functional differences in the long non-coding RNA *hota* in mouse and human. *PLoS Genet.* *7*, e1002071.
- Soshnikova, N., and Duboule, D. (2009). Epigenetic temporal control of mouse Hox genes in vivo. *Science* *324*, 1320–1323.
- Spitz, F., Gonzalez, F., Peichel, C., Vogt, T.F., Duboule, D., and Zákány, J. (2001). Large scale transgenic and cluster deletion analysis of the HoxD complex separate an ancestral regulatory module from evolutionary innovations. *Genes Dev.* *15*, 2209–2214.
- Suemori, H., and Noguchi, S. (2000). Hox C cluster genes are dispensable for overall body plan of mouse embryonic development. *Dev. Biol.* *220*, 333–342.
- Takahashi, N., Okamoto, A., Kobayashi, R., Shirai, M., Obata, Y., Ogawa, H., Sotomaru, Y., and Kono, T. (2009). Deletion of *Gtl2*, imprinted non-coding RNA, with its differentially methylated region induces lethal parent-origin-dependent defects in mice. *Hum. Mol. Genet.* *18*, 1879–1888.
- Tsai, M.C., Manor, O., Wan, Y., Mosammaparast, N., Wang, J.K., Lan, F., Shi, Y., Segal, E., and Chang, H.Y. (2010). Long noncoding RNA as modular scaffold of histone modification complexes. *Science* *329*, 689–693.
- Ulitsky, I., Shkumatava, A., Jan, C.H., Sive, H., and Bartel, D.P. (2011). Conserved function of lincRNAs in vertebrate embryonic development despite rapid sequence evolution. *Cell* *147*, 1537–1550.
- Yu, H., Lindsay, J., Feng, Z.P., Frankenberg, S., Hu, Y., Carone, D., Shaw, G., Pask, A.J., O'Neill, R., Papenfuss, A.T., and Renfree, M.B. (2012). Evolution of coding and non-coding genes in HOX clusters of a marsupial. *BMC Genomics* *13*, 251.
- Zacharek, S.J., Fillmore, C.M., Lau, A.N., Gludish, D.W., Chou, A., Ho, J.W., Zamponi, R., Gazit, R., Bock, C., Jäger, N., et al. (2011). Lung stem cell self-renewal relies on BMI1-dependent control of expression at imprinted loci. *Cell Stem Cell* *9*, 272–281.
- Zhao, J., Ohsumi, T.K., Kung, J.T., Ogawa, Y., Grau, D.J., Sarma, K., Song, J.J., Kingston, R.E., Borowsky, M., and Lee, J.T. (2010). Genome-wide identification of polycomb-associated RNAs by RIP-seq. *Mol. Cell* *40*, 939–953.